

Target and beam-target asymmetries for the $\gamma p \rightarrow \pi^0 \pi^0 p$ reaction

S. Garni,¹ V. L. Kashevarov,^{2,3,*} A. Fix,^{4,†} S. Abt,¹ F. Afzal,⁵ P. Aguar Bartolome,² Z. Ahmed,⁶ J. Ahrens,² J.R.M. Annand,⁷ H.J. Arends,² M. Bashkanov,⁸ R. Beck,⁵ M. Biroth,² N. Borisov,³ A. Braghieri,⁹ W.J. Briscoe,¹⁰ S. Cherepnaya,¹¹ F. Cividini,² C. Collicott,¹² S. Costanza,^{9,‡} A. Denig,² A.S. Dolzhikov,³ E.J. Downie,¹⁰ P. Drexler,^{2,13} L.V. Fil'kov,¹¹ S. Gardner,⁷ D.I. Glazier,^{7,8} I. Gorodnov,³ W. Gradl,² M. Günther,¹ D. Gurevich,¹⁴ L. Heijkskjöld,² D. Hornidge,¹⁵ G.M. Huber,⁶ A. Käser,¹ S. Kay,⁸ I. Keshelashvili,^{1,§} R. Kondratiev,¹⁴ M. Korolija,¹⁶ B. Krusche,¹ A. Lazarev,³ V. Lisin,¹⁴ K. Livingston,⁷ S. Lutterer,¹ I.J.D. MacGregor,⁷ R. Macrae,⁷ Y. Maghrbi,^{1,¶} D.M. Manley,¹⁷ P.P. Martel,^{2,18} J.C. McGeorge,⁷ D.G. Middleton,¹⁸ R. Miskimen,¹⁹ E. Mornacchi,² C. Mullen,⁷ A. Mushkarenkov,^{9,19} A. Neganov,³ A. Neiser,² M. Oberle,¹ M. Ostrick,² P.B. Otte,² B. Oussena,^{2,10} D. Paudyal,⁶ P. Pedroni,⁹ F. Pheron,¹ A. Polonski,¹⁴ A. Powell,⁷ S.N. Prakhov,²⁰ G. Ron,²¹ T. Rostomyan,^{1,**} A. Sarty,¹² C. Sfienti,² V. Sokhoyan,² K. Spieker,⁵ O. Steffen,² I.I. Strakovsky,¹⁰ I. Supek,¹⁶ A. Thiel,⁵ M. Thiel,² A. Thomas,² M. Unverzagt,² Yu.A. Usov,³ S. Wagner,² N.K. Walford,¹ D.P. Watts,⁸ J. Wettig,² M. Wolfes,² L.A. Zana,⁸ and F. Zehr¹

(A2 Collaboration)

¹Department of Physics, University of Basel, Ch-4056 Basel, Switzerland²Institut für Kernphysik, University of Mainz, D-55099 Mainz, Germany³Joint Institute for Nuclear Research, 141980 Dubna, Russia⁴Tomsk Polytechnic University, Tomsk, Russia⁵Helmholtz-Institut für Strahlen- und Kernphysik, University Bonn, D-53115 Bonn, Germany⁶University of Regina, Regina, SK S4S-0A2 Canada⁷SUPA School of Physics and Astronomy, University of Glasgow, Glasgow, G12 8QQ, UK⁸SUPA School of Physics, University of Edinburgh, Edinburgh EH9 3JZ, UK⁹INFN Sezione di Pavia, I-27100 Pavia, Pavia, Italy¹⁰Center for Nuclear Studies, The George Washington University, Washington, DC 20052, USA¹¹Lebedev Physical Institute, RU-119991 Moscow, Russia¹²Department of Astronomy and Physics, Saint Mary's University, E4L1E6 Halifax, Canada¹³II. Physikalisches Institut, University of Giessen, D-35392 Giessen, Germany¹⁴Institute for Nuclear Research, RU-125047 Moscow, Russia¹⁵Mount Allison University, Sackville, New Brunswick E4L1E6, Canada¹⁶Rudjer Boskovic Institute, HR-10000 Zagreb, Croatia¹⁷Kent State University, Kent, Ohio 44242, USA¹⁸Mount Allison University, Sackville, New Brunswick E4L3B5, Canada¹⁹University of Massachusetts, Amherst, Massachusetts 01003, USA²⁰University of California Los Angeles, Los Angeles, California 90095-1547, USA²¹Racah Institute of Physics, Hebrew University of Jerusalem, Jerusalem 91904, Israel

(Dated: today)

Background: Photoproduction of pion pairs allows the study of sequential decays of nucleon resonances via excited intermediate states. Such decays are important for complex states involving more than one quark excitation which de-excite in a two-step process. However, the analysis of multi-meson final states is difficult and generally relies on measurement of polarization observables.

Purpose: Experimental measurement and analysis of target and beam-target polarization observables of the $\gamma p \rightarrow \pi^0 \pi^0$ reaction.

Methods: Target (single) and beam-target (double) polarization asymmetries were investigated as a function of several parameters. The experiments were performed at the Mainz Microtron (MAMI) laboratory using circularly polarized photon beams and transversally polarized solid-butanol targets. The reaction products were analyzed with a near 4π solid-angle electromagnetic calorimeter composed of the Crystal Ball and TAPS detectors.

Results: The polarization observables studied were P_y (unpolarized beam, target polarized in the y direction) and P_x° (circularly polarized beam, target polarized in the x direction), which are similar to T (target asymmetry) and F (beam-target asymmetry) for single meson production. The asymmetries were analyzed with three independent methods, revealing systematic uncertainties. Some results are also given for the asymmetries P_x and P_y° which contribute only for three-body final states.

Conclusions: The measured observables allow some general conclusions to be drawn about the resonance content of the reaction amplitude. The $3/2^-$ partial wave shows a clear resonant behavior, attributed in the second resonance region to the sequential decay of the $N(1520)3/2^-$. The behavior of the $1/2^-$, $3/2^+$ partial waves is much smoother and the origin of a $3/2^+$ component at low energies is not well understood. The new data are important for future analyses of the partial wave structure of the $\pi^0 \pi^0$ photoproduction amplitude. However, further experimental results for the isospin dependence and the helicity decomposition of the reaction are needed.

I. INTRODUCTION

Photoproduction of pairs of pseudoscalar mesons from nucleons, in particular $\pi\pi$ [1–24] and $\pi\eta$ pairs (see [26] and Refs. therein for a summary and [27–30] for most recent results), has been studied intensively during the last two decades. Many data for angular, energy, and invariant mass distributions of the unpolarized cross sections as well as for some polarization observables have been collected for proton and quasi-free neutron targets and for the production of both charged and neutral mesons.

The purpose of many of these experiments is to extract the partial wave structure of the reaction amplitudes in order to study the contributions of nucleon resonances in the presence of non-resonant backgrounds. The main motivation is that excited nucleon states, due to their internal structure, can have much larger decay probabilities for sequential decays, involving intermediate states, than for direct decays to the nucleon ground state. This is obvious for higher lying states that have two independent excited quark model oscillator modes and de-excite in a two-step process [19]. However, already at fairly low excitation energies, e.g. for the $N(1520)3/2^-$ resonance, significant branching ratios to sequential $\pi\pi$ decays via the $\Delta(1232)3/2^+$ state have been observed [4, 33].

The most interesting but probably the least comprehensible channel in the production of pion pairs is $\pi^0\pi^0N$. Experimental data for this final state, in particular in the second and third resonance region are rapidly being accumulating. The investigation of this reaction, which was not accessible to early experiments based on magnetic momentum analysis of charged pions, was pioneered by the DAPHNE [1] and TAPS [2] experiments at MAMI with measurements of total cross sections. Subsequently many further results have been reported for free proton and quasi-free neutron targets with and without polarization degrees of freedom [3–19].

It has been frequently emphasized that this channel is especially convenient for studying nucleon resonances, since in contrast to other channels with at least one charged pion, only few reaction mechanisms contribute to $\pi^0\pi^0$ photoproduction. Other contributions such as Δ Kroll-Ruderman term, pion-pole terms, ρ photoproduction etc. are forbidden. However, these peculiarities

also represent a challenge to studying dynamical properties of this channel using specific models. In absence of the well understood Born terms, mentioned above, other background terms, whose nature is not well studied and which are usually very model dependent, become relatively more important. This makes models for $\pi^0\pi^0$ to some extent unreliable and is the main reason why significant qualitative differences between the results of different analyses of $\pi^0\pi^0$ photoproduction still exist. Interestingly, the model interpretation of this reaction is much less advanced than for the $\pi^0\eta$ final state which is more strongly dominated by a few resonant terms [28–31].

Some analyses [10, 14, 33] point to an important role of the states with spin $J = 3/2$ in $\pi^0\pi^0$ photoproduction, not only in the vicinity of $N(1520)3/2^-$ but also at much lower energies. In Ref. [10] this conclusion is based on a global fit to different reaction channels, such as $\gamma p \rightarrow \pi^0 p$ $\pi^- p \rightarrow \pi^0\pi^0 p$, etc. This analysis claims evidence for a dominant contribution from the partial wave with isospin $I = 3/2$ and spin-parity $3/2^-$ in $\pi^0\pi^0$ photoproduction and assigns the double-hump structure of the total cross section in the second and third resonance regions to an interference of this wave (dominated by the $\Delta(1700)3/2^-$ resonance) with other contributions in particular from the $N(1520)3/2^-$ state. In a later analysis [18] also significant contributions from the $N(1680)5/2^-$ state to the third resonance peak were claimed.

In Ref. [14] a partial wave expansion of the amplitude was analyzed. The measured moments W_{LM} of the angular distribution were fitted with this expansion. They represent the final state partial wave contributions with total momentum J and projection M on the normal to the plane spanned by the momenta of the final particles [25]. It was shown that in the region up to $E_\gamma = 800$ MeV, where only the lowest partial waves with $J \leq 3/2$ are expected to be important, the qualitative features of the moments W_{LM} may unambiguously be interpreted in terms of the corresponding partial amplitudes. This allows rather firm conclusions about the dynamical content of the reaction to be drawn. In particular, it was found that the amplitude with $J^P = 3/2^+$ may be as important as that with $J^P = 3/2^-$. The problem behind this finding is that it is difficult to explain the origin of such a strong contribution of the $3/2^+$ wave. Therefore, although the phenomenological model with a large $3/2^+$ wave contribution explains rather well the observed angular and energy distributions in the reaction $\gamma p \rightarrow \pi^0\pi^0 p$ [14] the mechanism of the $\pi^0\pi^0$ production is still not well understood.

Better insight into details of the photoproduction of π^0 pairs requires the measurement of further observables, which can better constrain the model analyses. Of special interest are polarization observables because through interference terms they are sensitive to contributions from small reaction amplitudes. To date, besides the unpo-

* Electronic address: kashev@kph.uni-mainz.de

† Electronic address: fix@mph.phtd.tpu.ru

‡ Also at: Dipartimento di Fisica, Università di Pavia, I-27100 Pavia, Italy

§ Present address: Institut für Kernphysik, FZ Jülich, 52425 Jülich, Germany

¶ Present address: College of Engineering and Technology, American University of the Middle East, Kuwait

** Present address: Department of Physics and Astronomy, Rutgers University, Piscataway, New Jersey, 08854-8019

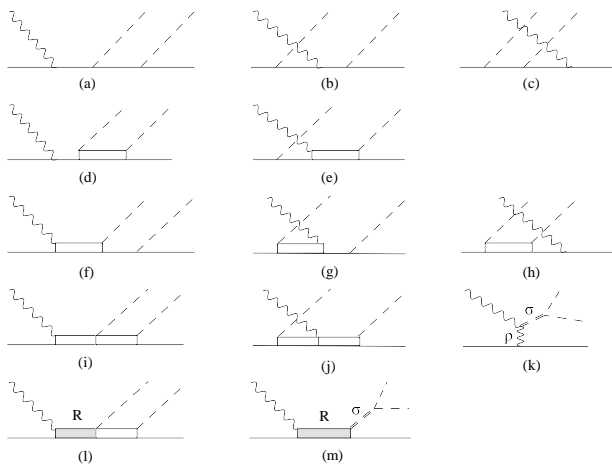


FIG. 1. Diagrams for the reaction $\gamma p \rightarrow \pi^0 \pi^0 p$ used in the present work. The empty rectangles represent the $\Delta(1232)$. Other resonances in the s channel are represented by shaded rectangles.

larized cross section, experimental results for linear and circular beam asymmetries [6, 12, 13, 15, 17, 18] and beam-target asymmetries [8] have already been collected and partially been analyzed within different models [32–36]. It will certainly not be possible to do a ‘complete’ experiment, leaving no ambiguities, for the production of pseudoscalar meson pairs. This problem has not even been solved up to now for single π^0 photoproduction and there are significantly more degrees of freedom for pion pairs. While 8 observables need to be measured as a function of two kinematic variables for a unique solution for single pseudoscalar meson production [37], pseudoscalar pairs require 8 observables to be measured as a function of five kinematic variables just to fix the magnitudes of the amplitudes and require a total of 15 observables to also determine the phases [38].

However, in some cases the partial wave content can be studied using a restricted number of observables while making some physically reasonable general assumptions about the production mechanisms. Some of observables have already been measured and presented in earlier papers cited above. In the present work we expand the set of observables with the target and the beam-target asymmetries, which were not experimentally investigated before now. An update of the model from [34] was used for the interpretation of the data. The diagrams considered in this model are summarized in Fig. 1. A new fit of the model to the recent data base for $\gamma N \rightarrow N \pi \pi$ has been made made.

II. GENERAL FORMALISM

The general formalism for the photoproduction of pseudoscalar meson pairs from nucleons was developed in Refs. [38] and [39], where the formulae for different polar-

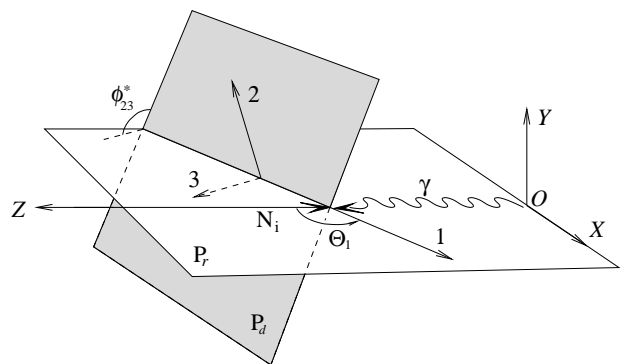


FIG. 2. Definition of the coordinate system used in the present work. The azimuthal angle ϕ_{23}^* is defined in the center of mass system of the particles 2 and 3 with the z -axis opposite to the momentum of the particle 1 and y -axes parallel to OY . It is equal to the angle between the reaction plane P_r and the decay plane P_d .

ization observables were also presented. In the following we denote the final-state particles as 1, 2, and 3 and consider the partition $1 + (23)$. Because the two pions are identical particles, there are two independent sets of variables, corresponding to the numbering $1 + (23) = p + (\pi \pi)$ and $\pi + (\pi p)$. The coordinate system is shown in Fig. 2. The Z axis is directed along the photon momentum. The X and Y axes are chosen such that the momentum of the particle 1 has a positive X -projection and is orthogonal to the Y -axis. As independent kinematic variables we choose the solid angle $\Omega_1 = (\Theta_1, \Phi_1 = 0)$ of the particle 1, the solid angle $\Omega_{23}^* = (\theta_{23}^*, \phi_{23}^*)$ of the particle 2 in the center-of-mass of the pair (23) and the corresponding invariant mass M_{23} .

If the target nucleon is transversally polarized and the incident photon beam is circularly polarized the cross section may be written in the form (see Eq. (57) of Ref. [39])

$$\begin{aligned} \frac{d\sigma}{d\Omega_1 dM_{23} d\Omega_{23}^*} &= \frac{d\sigma_0}{d\Omega_1 dM_{23} d\Omega_{23}^*} \left\{ 1 + P_{\odot} T_{00}^c \right. \\ &\quad - \frac{1}{\sqrt{2}} P_T [T_{11}^0 \cos \phi_s + S_{11}^0 \sin \phi_s \\ &\quad \left. + P_{\odot} (T_{11}^c \cos \phi_s + S_{11}^c \sin \phi_s) \right\}, \end{aligned} \quad (1)$$

where the unpolarized differential cross section is denoted as σ_0 . The values of P_T and $|P_{\odot}|$ describe the degree of nucleon polarization along the direction determined by the angle $\Omega_s = (\theta_s = \frac{\pi}{2}, \phi_s)$ and the degree of photon circular polarization, respectively. The circular photon asymmetry T_{00}^c was already investigated in detail in Refs. [12, 13, 15] and is therefore excluded from the present study. As is seen from Eq. 1, for the totally exclusive five-fold cross section, there are two independent transverse target asymmetries (T_{11}^0 and S_{11}^0) and two independent beam-target asymmetries (T_{11}^c and S_{11}^c). They

TABLE I. Polarization observables measured in the present paper. In parentheses the corresponding notations from Ref. [38] are given.

Beam	Target	
	x	y
–	$T_{11}^0(P_x)$	$S_{11}^0(P_y)$
c	$T_{11}^c(P_x^\odot)$	$S_{11}^c(P_y^\odot)$

are related to those introduced in Ref. [38] by

$$T_{11}^0 = -P_x, \quad S_{11}^0 = -P_y, \quad T_{11}^c = -P_x^\odot, \quad S_{11}^c = -P_y^\odot. \quad (2)$$

The corresponding semi-exclusive cross sections may be obtained easily from (1) via appropriate integration. In particular, if one integrates over ϕ_{23}^* , the terms proportional to T_{00}^c , T_{11}^0 , and S_{11}^c vanish exactly, so that the final expression reads

$$\frac{d\sigma}{d\Omega_1 dM_{23}} = \frac{d\sigma_0}{d\Omega_1 dM_{23}} \left\{ 1 - \frac{1}{\sqrt{2}} P_T [\tilde{S}_{11}^0 \sin \phi_s + P_\odot \tilde{T}_{11}^c \cos \phi_s] \right\}, \quad (3)$$

where \tilde{T}_{11}^c and \tilde{S}_{11}^0 are the corresponding partially integrated (semi-exclusive) observables.

Table I summarizes how the asymmetries discussed above can be separated by a proper choice of the photon and proton polarization parameters. The observables S_{11}^0 and T_{11}^c are similar to the ordinary T and F asymmetries used for single pion photoproduction.

III. EXPERIMENTAL SETUP

The experiment was performed at the MAMI C accelerator in Mainz [40] using the Glasgow-Mainz tagged photon facility [41–43]. The reaction $\gamma p \rightarrow \pi^0 \pi^0 p$ was measured using the Crystal Ball (CB) [44] as the central calorimeter and TAPS [45, 46] as a forward detector. The CB detector is constructed as a sphere of 672 optically insulated NaI(Tl) crystals, pointing toward the center of the sphere. The crystals are arranged in two hemispheres that cover 93% of the full solid angle. For charged-particle identification a barrel of 24 scintillation counters, the Particle Identification Detector (PID) [47], and two multiple wire proportional chambers (MWPC) [48] surrounded the target. The forward angular range $\theta = 5-20^\circ$ was covered by the TAPS calorimeter [45, 46], that was arranged in a plane consisting of 384 hexagonally shaped BaF₂ detectors. A 5-mm thick plastic scintillator in front of each module allowed charged particles

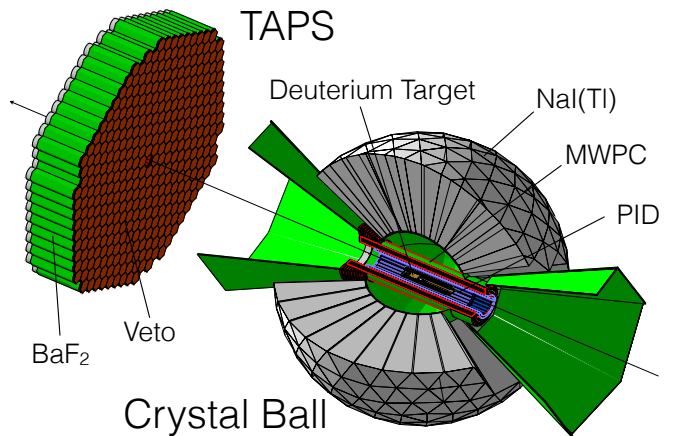


FIG. 3. (Color online) Setup of the electromagnetic calorimeter combining the Crystal Ball and TAPS detectors. Only three quarters of the CB are shown. For charged particle identification mounted inside the CB were the Particle Identification Detector (PID) and multiple wire chambers (MWPC) and in front of TAPS the TAPS Charged-Particle Veto (CPV) detector. The beam enters from the bottom right corner of the figure, the target was placed in the center of the CB

to be identified. The solid angle covered by the Crystal Ball and TAPS detection system is nearly 97% of 4π sr. More details on the energy and angular resolution and particle identification of the device are given in Refs. [49–53].

For the measurements discussed in this work longitudinally polarized electron beams with energies of 1558 MeV and polarization degrees of $\approx 80\%$ were used. The polarization of the electron beam was measured in special runs close to the electron source after the Linac accelerator at beam energies of 3.65 MeV with Mott scattering and it was continuously monitored with Møller scattering of the electrons from the ferromagnetic radiator foil (Vacoflux50, 10 μm thickness). The longitudinal polarization of the electrons was transferred to circular polarization of the photons according to [54]:

$$P_\gamma = P_{e^-} \cdot \frac{4x - x^2}{4 - 4x + 3x^2}, \quad (4)$$

where P_{e^-} and P_γ are the degrees of polarization of the electrons and the photons, respectively, and $x = E_\gamma/E_{e^-}$. The quasi-monochromatic photon beam covered the energy range from 450 to 1450 MeV. The circular polarization depends on the photon energy (Eq. (4)) and increased from $\approx 50\%$ at 450 MeV to $\approx 80\%$ at 1450 MeV.

The experiment required transversely polarized protons, which were provided by a frozen-spin butanol (C₄H₉OH) target. A specially designed ³He/⁴He dilution refrigerator was built for polarization measurements with the CB detector. The target was cooled down to ≈ 20 mK in a strong magnetic field of ≈ 2.5 T. Dynamic Nuclear Polarization (DNP) was used to transfer the electron polarization to the free protons, bound in the bu-

tanol molecules, by use of radio-frequency fields. When the required polarization was reached, the magnet with the large field was removed and replaced by a small superconducting holding coil (0.45 T), which allowed the target to be moved into the center of the main detector. The holding coil was a four layer saddle coil which operated at a current of 35 A and held the transverse polarization with a relaxation time of around 1500 h. The low material budget of this coil guaranteed that the effects on the critical detection of charged particles (recoil protons) would be small. These effects were modeled using a Monte Carlo (MC) simulation. The cylindrical target container (2 cm long \times 2 cm diameter) was filled by 2 mm diameter butanol spheres with a filling factor around 60%. Typical polarization degrees obtained (averaged over the exponential decay due to the relaxation time) during the present measurements were around 70%. More details about construction and operation of the target are given in Ref. [55].

The use of butanol targets has the disadvantage that signals from unpolarized nucleons bound in the carbon and oxygen nuclei of the molecule dilute the polarization signal. The elimination of such backgrounds (as discussed in detail in the next section) requires the additional measurement of the reaction from the free proton using liquid hydrogen (LH₂) targets and from solid carbon targets. For the latter, a special solid carbon foam was used that can be produced so that it matches exactly the geometry and the density of carbon nuclei in the butanol target (in fact, the density was also corrected to represent the much less abundant oxygen nuclei in butanol). In total, four different beam times were analyzed for the present results, which are summarized in Tab. II.

	Run I	Run II	Run III	Run IV
Target type	LH ₂	C ₄ H ₉ OH	C ₄ H ₉ OH	C-foam
target length [cm]	10	2	2	2
target radius [cm]	4	2	2	2
density [barn ⁻¹]	0.421	0.092	0.092	0.057
e ⁻ energy [MeV]	1558	1558	1558	1558
beam-radius [cm]	1.3	1.3	1.3	1.3
multiplicity trigger	M3+	M2+	M2+	M2+
CB sum trigger [MeV]	360	350	300	350
MWPC	no	no	yes	yes
PID	yes	yes	no	yes

TABLE II. Main parameters of the experimental sets. The surface density in barn⁻¹ is given in nuclei/barn for the LH₂ target and the carbon-foam target, but in molecules/barn for the butanol targets. The effective surface densities of free protons in the butanol targets are a factor of 10 higher. The beam radius refers to the radius of the photon-beam spot size on the target.

Two production beam times with the polarized butanol target and one with a liquid hydrogen and one with a carbon target for background elimination were taken. The trigger for all measurements was based on a multiplicity condition for hits in the calorimeter. For this purpose

both CB and TAPS were subdivided into logical sectors (see [49–53] for details). However, this condition was not critical for the present analysis. Only the measurement with the liquid hydrogen target used a multiplicity-three trigger, the other used multiplicity-two triggers and a final state that requires four detected photons is not biased by any of these conditions. In addition, an analog-sum threshold for the total energy deposition in the CB between 300 and 360 MeV was required.

There are, however, two factors which complicated the analysis. The first is the difference in target length between the measurement with the liquid hydrogen target and the measurements with the solid targets. The resolution for invariant and missing masses (see next section), used to separate signal from background, depends significantly on target length (due to the uncertainty in the unmeasured reaction vertex). Results from the hydrogen measurement could therefore not be directly compared to the solid state targets. Furthermore, the particle identification detectors inside the CB, the PID and the MWPCs, were not fully operational during all measurements. The MWPCs were not active for the measurement with the liquid hydrogen target and for one of the beam-time periods with the butanol target (II), while the PID had several dead channels for the other butanol measurement (III). This required some very detailed data analysis which is discussed in the next section.

IV. DATA ANALYSIS

The data were analyzed in several different ways. All analyses accepted only events with five hits (candidates for four photons and one proton) in the combined calorimeter. The differences concerned the identification of the recoil protons and the treatment of the carbon/oxygen background in the asymmetry ratios.

In all analyses photons and protons in TAPS were identified with the standard analysis methods for this detector using the response of the TAPS CPV detector, a pulse shape analysis (PSA), and a time-of-flight (ToF) versus-energy analysis as described in detail in Refs. [16, 51–53].

Charged particles hitting the CB can be identified in principle from the response of the PID and/or the MWPCs. There was, however, the problem that the MWPCs were not activated for Runs I and II and the PID could not be used for Run III. Therefore the following analysis strategies were adopted.

All four runs were first analyzed ignoring the information from the PID and the MWPCs and instead accepting only hits with one responding NaI crystal (hit multiplicity one) in the CB as protons. In the energy range of interest, photon hits almost always activate two or more modules. This analysis has the advantage that it minimizes instrumental asymmetries, but it significantly reduces counting statistics because only a fraction of proton hits are multiplicity-one hits. Furthermore, it suffers from low resolution for the proton angles, which can be

determined much more precisely when the MWPCs are used. All results from this analysis were averaged for the two butanol beam times (Runs II, III in Tab. II).

The other analyses used either the PID or the MWPCs for proton identification in the CB. The PID was used for Run I and Run II, the MWPCs for Run III, and the carbon-background measurement was in one case analyzed with the PID, ignoring the MWPC information and vice versa in the other case. However, it turned out that for the analysis of Run II (first butanol beam time) the efficiency calibration of the PID was not good enough to remove all instrumental effects for the azimuthal distribution of the recoil protons. This was no problem for the extraction of the double-polarization asymmetry P_x^\odot , because such artefacts cancel in the difference of positive and negative beam polarization. However, the target asymmetry P_y was affected by it. Therefore, the analyses using the charged particle identification detectors could be averaged over both butanol beam times for the P_x^\odot observable, but only Run III with the MWPCs was used for the target asymmetry P_y .

The other difference between the analyses was the treatment of the unpolarized background from the carbon and oxygen nuclei in the butanol target. The asymmetries have been evaluated from:

$$P_y \sin(\phi_s) = \frac{1}{P_T} \frac{d\sigma^\uparrow(\phi_s) - d\sigma^\downarrow(\phi_s)}{d\sigma^\uparrow(\phi_s) + d\sigma^\downarrow(\phi_s)} \quad (5)$$

and from:

$$P_x^\odot \cos(\phi_s) = \frac{1}{P_T} \frac{1}{P_\odot} \frac{d\sigma^+(\phi_s) - d\sigma^-(\phi_s)}{d\sigma^+(\phi_s) + d\sigma^-(\phi_s)}, \quad (6)$$

with

$$\begin{aligned} d\sigma^\uparrow &\equiv d\sigma^{\uparrow+} + d\sigma^{\uparrow-}, & d\sigma^\downarrow &\equiv d\sigma^{\downarrow+} + d\sigma^{\downarrow-} \\ d\sigma^+ &\equiv d\sigma^{\uparrow+} + d\sigma^{\downarrow-}, & d\sigma^- &\equiv d\sigma^{\downarrow+} + d\sigma^{\uparrow-} \end{aligned} \quad (7)$$

where P_T and P_\odot are the polarization of the target (transverse) and beam (circular), respectively. The cross sections refer to the different orientations of the target spin (\uparrow, \downarrow) and the two polarization states of the beam ($+, -$).

Backgrounds from the non-polarized nucleons bound in the carbon and oxygen nuclei of the butanol targets cancel in Eqs. 5,6 in the numerator, but they contribute in the denominator. This background contribution can be treated in two different ways. Either, the contribution from the nucleons bound in carbon/oxygen nuclei is removed with the help of the background measurement using a carbon foam target (the small contribution from oxygen was approximated by an $A^{2/3}$ scaling law [56]). Alternatively, the results from the measurement with a liquid hydrogen target, which are free of such backgrounds, can be used in the denominator. In the present work both methods were exploited for the analyses using the charged particle identification detectors, but only the carbon subtraction method was used for the analysis relying on proton identification via hit multiplicity.

Analyses	(1)	(2)	(3)
proton denominator	MWPC/(PID) carbon sub.	MWPC/(PID) hydrogen norm.	hit multiplicity carbon sub.

TABLE III. Characteristics of the analyses (1), (2), (3). First line: identification of recoil proton by charged particle detectors or hit multiplicity in CB. Second line: treatment of non-polarized background, carbon subtraction or denominator of asymmetry from measurement with liquid hydrogen target.

The analysis strategies are summarized in Tab. III. The advantage of the analyses using the carbon subtraction is that many systematic uncertainties cancel in the ratios of Eqs. 5,6. The advantage of the normalization to the results from a hydrogen target in Eqs. 5,6 is the elimination of unpolarized backgrounds.

The main steps for the identification of decay photons and recoil protons from the $\gamma p \rightarrow p\pi^0\pi^0$ reaction were similar to the methods used in [15, 16, 57]. In the first step, hits in the calorimeter were designated as ‘charged’ or ‘neutral’ using either the information from the TAPS CPV and the PID and/or the MWPCs surrounding the target (analyses (1),(2)) or the hit multiplicity (analysis (3)).

In the next step, the four photon candidates were analyzed. The relative timing between the photons was measured for photon pairs in TAPS with a resolution (FWHM) of ≈ 0.5 ns, for photon pairs with one photon in TAPS and one in CB with ≈ 1.5 ns, and for pairs in CB with ≈ 2.5 ns. Cuts were applied to the relative timing, however they had very little effect. The initial spectra already had a very low background level and were background free after the subsequent kinematic cuts were applied. The timing of the photons was also used to remove background from random tagger-calorimeter coincidences. In this case the resolution was ≈ 1 ns for the TAPS-tagger coincidence and ≈ 1.5 ns for the CB-tagger coincidence. The random background was removed as in previous analyses (see e.g. [51]) by a cut on the prompt time peak and a side-band subtraction of the flat background.

A χ^2 analysis was used to identify the most probable out of the three combinatorial possible combinations of the four photons from the decay of two π^0 mesons. The χ^2 was defined by

$$\chi^2(k) = \sum_{i=1}^2 \left(\frac{m_{\pi^0} - m_{i,k}}{\Delta m_{i,k}} \right)^2 \quad \text{with } k = 1, \dots, 3, \quad (8)$$

where m_{π^0} is the nominal π^0 mass, the $m_{i,k}$ are the invariant masses of the i -th pair in the k -th permutation of the hits and $\Delta m_{i,k}$ is the corresponding uncertainty from the experimental energy and angular resolution. Both were computed event-by-event. Only the combination with the smallest χ^2 was analyzed further.

In the next step the invariant masses of these photon pairs were analyzed. Figure 4 shows some typical exam-

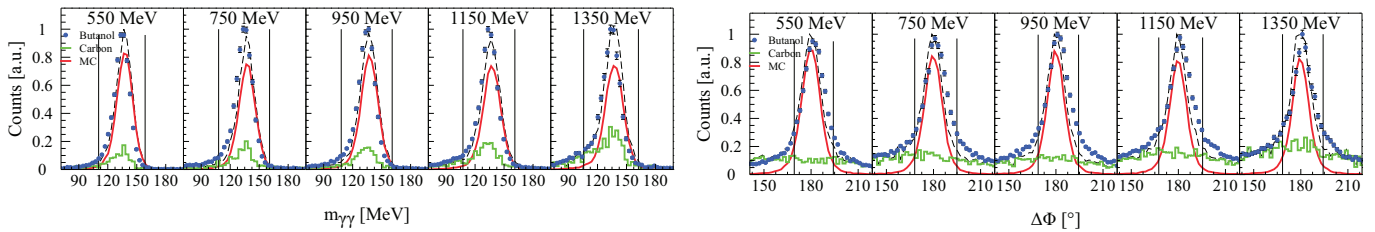


FIG. 4. (Color online) Left hand side: invariant masses for different ranges of incident photon energy (indicated in figure). Points (blue) with error bars: measured butanol data. Solid (red) lines: hydrogen data corrected by MC simulation for resolution effects (see text). Solid (green) lines: background from carbon data. Dashed (black) lines: sum of hydrogen and carbon data. Vertical lines indicate cuts applied to invariant mass. The cuts on coplanarity and missing mass are applied to this spectra. Right hand side: coplanarity spectra (see text). Same notation as left hand side. Cuts on invariant mass are applied. All butanol data from Run III, analyzed with charged particle detectors (MWPCs). Results from Run II (PID) are not significantly different for the invariant mass, but have less background in coplanarity, in particular outside the peak region.

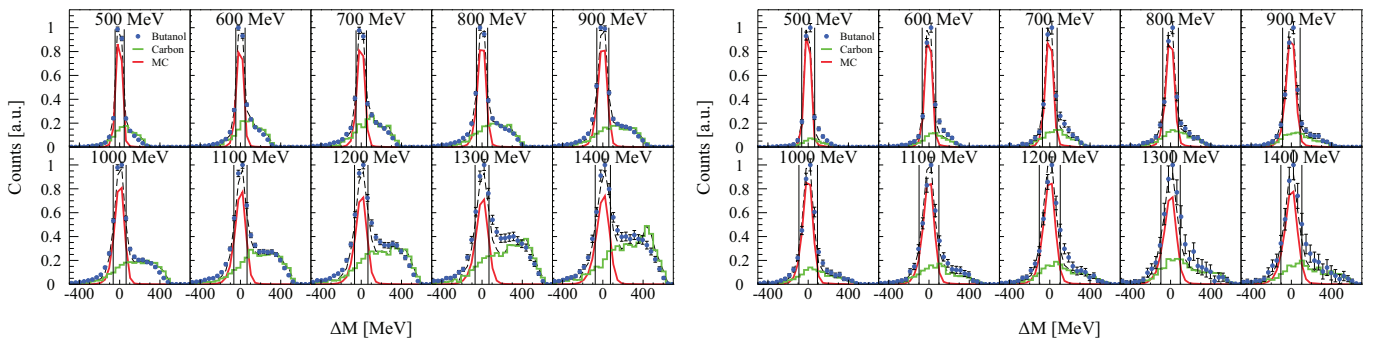


FIG. 5. (Color online) Missing mass spectra for different ranges of incident photon energy. Notation as in Fig. 4. Left hand side: Run III (charged particle identification with MWPCs), right hand side: Run II (charged particle identification with PID). Vertical lines indicate cuts applied to missing mass. The invariant mass cuts are applied to this spectra.

ples of the invariant mass of the photon pairs obtained from Run III with the butanol target compared to the results measured with the carbon foam and hydrogen target. The analysis was done with the use of the MWPCs for identification of the proton (results from Run II with usage of the PID are very similar). The counts from the three different targets (butanol, carbon, hydrogen) have been absolutely normalized by the target densities, integrated photon fluxes, and the detection efficiencies obtained from Monte Carlo (MC) simulations done with the Geant4 code [58]. The simulations included known inefficiencies of the charged particle detectors. The results from the measurement with the hydrogen target could not be compared directly to the other two targets because the length of the hydrogen target (see Tab. II) was five times the length of the butanol and carbon targets which affects the experimental resolution because the reaction vertex is not known. Therefore, in a first step the results from the hydrogen target were compared to a MC simulation using the actual length of that target. Almost perfect agreement of the line shape was found. Subsequently, the MC simulation for the hydrogen target was repeated for the target length of the butanol target and the simulated line shape was normalized with the

measured count rate of the hydrogen target. This was also done for the kinematical spectra (coplanarity and missing mass) discussed below. After this correction the invariant-mass line shapes for the three targets were very similar as expected because nuclear Fermi motion does not affect invariant masses. The figure shows only a few examples of these spectra for different energy bins. The actual analysis was carried out using finer bins of energy and also as a function of the polar angle of the recoil proton. The sum of the absolutely normalized count rates for the hydrogen and carbon target reproduces very well the measured yield for the butanol target. The vertical lines in the figure indicate the cuts applied in further analysis.

After the invariant-mass analysis, the mass of the π^0 meson was used as a constraint to improve the resolution in further kinematical analyses. Since the angular resolution of the detector is much better than the energy resolution this was simply done by replacing the measured energies of the decay photons E_{γ_1} , E_{γ_2} by

$$E'_{\gamma_1, \gamma_2} = \frac{m_{\pi^0}}{m_{\gamma_1 \gamma_2}} E_{\gamma_1, \gamma_2}, \quad (9)$$

where m_{π^0} is the mass of the π^0 meson and $m_{\gamma_1 \gamma_2}$ is the

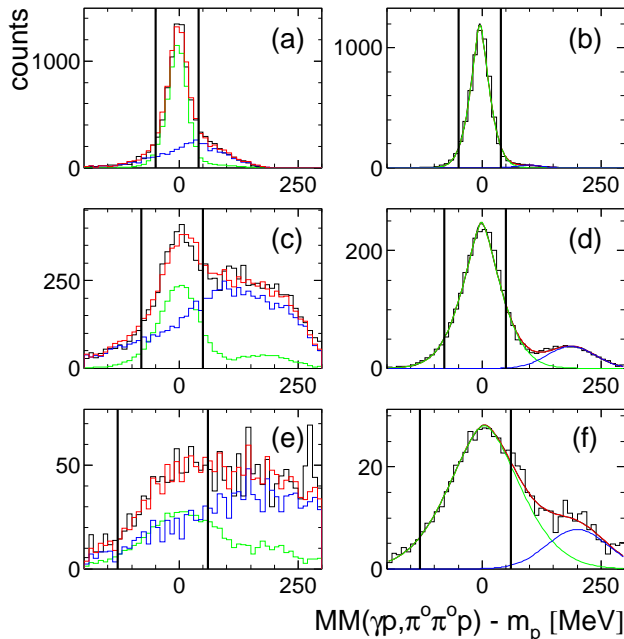


FIG. 6. (Color online) Left hand side ((a),(c),(e): typical missing mass spectra from analysis (3) with proton identification by hit multiplicity for photon energies around 600, 900, and 1400 MeV (bin widths ± 50 MeV). Black histograms: butanol data, green histograms: hydrogen data, blue histograms: carbon data, red histograms: sum of hydrogen and carbon data. Right hand side ((b),(d),(f)): missing mass spectra for hydrogen target. Black histograms: measured data, green lines: MC simulation of $\pi^0\pi^0$ final state, blue lines: MC simulation of background from $3\pi^0$ final states, red lines: sum of signal and background from MC.

invariant mass of the photon pair with originally measured energies.

The first kinematic condition that was checked is the coplanarity of the two-pion system and the recoil proton. Due to momentum conservation, the difference in the azimuthal angle $\Delta\Phi$ between the $\pi^0\pi^0$ pair and the recoil nucleon must be 180° . This is normally not the case when additional particles have escaped detection (for example from triple-pion final states). The result of this analysis for Run III (Run II is very similar) is shown in Fig. 4 (right hand side) together with the applied cuts. Again the normalized results from the hydrogen and carbon target add up to the data obtained with the butanol target. In this case the carbon background is rather flat due to the large effect from nuclear Fermi motion.

Even more efficient is the analysis of the missing mass for which the recoil proton, although detected, is treated as a missing particle and its four momentum is reconstructed from the reaction kinematic using

$$\Delta M = \left| P_\gamma + P_N - P_{\pi_1^0} - P_{\pi_2^0} \right| - m_N, \quad (10)$$

where P_γ , P_N , $P_{\pi_1^0}$, $P_{\pi_2^0}$ are the four-momenta of the in-

cident photon, the initial state nucleon (at rest) and the two pions. The nucleon mass m_N was subtracted so that true $\gamma N \rightarrow N\pi^0\pi^0$ events were expected at $\Delta M = 0$. The result of this analysis is shown in Fig. 5 for the analyses of Run III (left hand side) and Run II (right hand side). In both cases the normalized yields from the hydrogen and carbon targets add up to the butanol data. The background suppression is better for the measurement using the PID detector (Run II) than with the MWPCs (Run III). However, as mentioned earlier, the response for the proton detection was more isotropic in the azimuthal angle Φ for the measurement with the MWPCs. These spectra (again analyzed with finer energy bins as a function of the proton polar angle) were used to subtract the carbon background in analysis (1) (see table III).

In the case of analysis (2) the carbon background played no role because it cancels in the numerator of the asymmetry and the measurement with the hydrogen target was directly used for normalization.

Missing mass spectra for analysis (3), using the hit multiplicity for proton identification, are summarized in Fig. 6. The left-hand side of the figure shows the comparison of the yields from the butanol, carbon, and hydrogen targets. In this case the three yields were not absolutely normalized but the relative contribution of the carbon and hydrogen target was fitted so that the sum reproduced the butanol measurement. The fitting was only done in the signal missing-mass range indicated by the vertical lines. The right-hand side of the figure shows the experimental results for the hydrogen target compared to MC simulated responses for double π^0 production and background from $3\pi^0$ final states. Also in this analysis background from carbon was subtracted and the background from $3\pi^0$ production does not significantly intrude into the missing mass range selected by the cuts. Some results for the two asymmetries P_x and P_y^\odot , which were not investigated with analysis (1) and (2), were obtained from this analysis.

V. SYSTEMATIC UNCERTAINTIES

Systematic uncertainties arise from several sources with different impact on the analysis strategies and the investigated observables. The measurement of the target polarization degree P_T affects all measured asymmetries in the same way. The polarization of the target was regularly reversed in order to reduce the uncertainty. The systematic uncertainty in the target polarization was estimated from the NMR measurements to be $\approx 4\%$. The polarization degree of the photon beam affects only the measurement of the P_x^\odot and P_y^\odot beam-target asymmetries. This was estimated from the Mott measurements to be $\approx 3\%$. The measurement of the various asymmetries is also affected by variations in the azimuthal efficiency of the detectors. The detector response was MC simulated and corrected. Residual effects were investigated in two ways. The target asymmetry was determined indi-

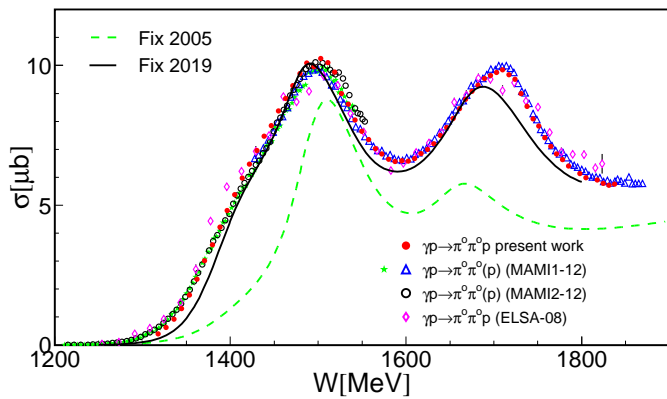


FIG. 7. (Color online) Total cross section for the $\gamma p \rightarrow p\pi^0\pi^0$ reaction as function of the total cm energy W . Data from the present analysis (red, filled spheres) for the measurement with a liquid hydrogen target compared to previous results from the Mainz MAMI facility (blue, open triangles and green stars [14]; black open circles [13]) and the Bonn ELSA facility [11]). The (green) dashed line is the prediction for the total cross section from the MAID model [34]. The (black) solid line is an update of the same model using nucleon resonance parameters from the 2018 PDG compilation [60] and a refit of the model to all available data.

vidually for both directions of target polarization by an analysis of the azimuthal angular distributions replacing $d\sigma(\phi_s)^\downarrow$ by $d\sigma(\phi_s + \pi)^\uparrow$ in Eq. (5) etc. In the absence of instrumental effects both results must agree. Furthermore, the target asymmetries were fitted with an incorrect $\cos(\phi_s)$ angular dependence in which case they must vanish unless instrumental asymmetries contribute. Both conditions were fulfilled within statistical uncertainties for Run III using the MWPCs, but not for Run II using the PID. Therefore, Run II, which was also inferior in terms of counting statistics, was discarded for the target asymmetries. Such effects are not significant for the beam-target asymmetries. They cancel in the subtraction of the count rates from the two beam polarizations.

Further systematic uncertainty arises from either the subtraction of the carbon background in analyses (1,3) or the normalization to hydrogen data in analysis (2). When the denominator of Eqs. 5,6 is taken from the measurement with a hydrogen target all cross sections must be absolutely normalized (beam flux, target density, detection efficiency). For the subtraction of the carbon contribution the relative normalization of the butanol and carbon data matters. The target size and density of the butanol and carbon targets were well matched (the density of the carbon foam was identical to the density of carbon nuclei in the butanol target including a correction for oxygen nuclei). Also the experimental conditions (trigger, thresholds) were kept as similar as possible, so that many effects canceled without requiring a precise normalization. The largest effects were then due to the exact reproduction of line shapes in the missing-mass spectra used to eliminate the background. This depends on the

methods used to identify the recoil proton (PID, MWPCs, or hit multiplicity, see Figs. 5,6).

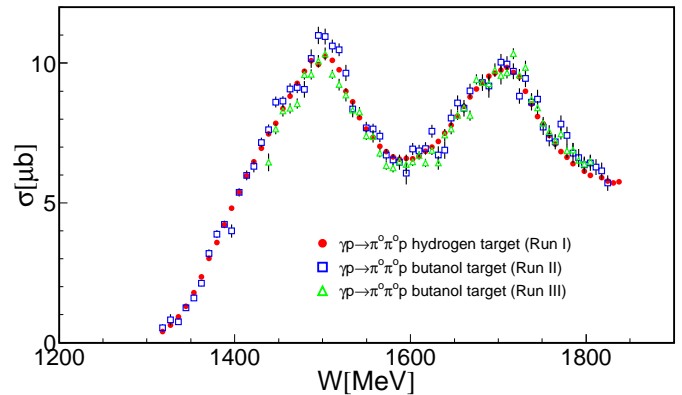


FIG. 8. (Color online) Comparison of the total cross section for the hydrogen target (Run I) from the present analysis to the total cross sections for the $\gamma p \rightarrow p\pi^0\pi^0$ extracted from the measurements with the butanol targets (Runs II,III) after subtraction of the carbon background from Run IV.

The absolute normalization of the data included not only target density and photon fluxes. Also the instrumental acceptance and detection efficiency were tested by an analysis of the total cross section of the $\gamma p \rightarrow p\pi^0\pi^0$ reaction. Fig. 7 shows the total cross section of this reaction from the present measurement with the hydrogen target (Run I) compared to previous results. The statistical quality of the present data is even better than that of the previous measurements. No significant systematic deviations were observed. This is not trivial because for the previous MAMI results [13, 14] only detection of the four π^0 decay photons, with subsequent invariant-mass and missing-mass analyses, was required. In contrast to the present analysis, recoil protons were ignored in these measurements. The previous analysis strategy avoided all problems with proton detection efficiency. However, for the measurements with the butanol target coincident detection of recoil protons is very useful for background elimination. Therefore, the hydrogen data were analyzed in coincidence with protons using the charged particle detectors (PID, CPV) Tof-versus-energy, and PSA.

The curves in Fig. 7 show the predictions of the isobar model from Ref. [34], which was used as basis of the analysis of the data. The dashed line shows the result from Ref. [34], the solid line the update with resonance parameters from the most recent PDG (Particle Data Group) [60] compilation and a refit to double pion production data. This refit describes the data much better than the original version of the model.

Figure 8 shows a comparison of the total cross section from the present analysis of the measurement with the hydrogen target (Run I) to the results from the two measurements (Run II, III) with the butanol target after subtraction of the carbon background determined with Run IV. For these analyses proton identification was done

with the charged particle detectors active for runs I,II,III
(see Tab. II).

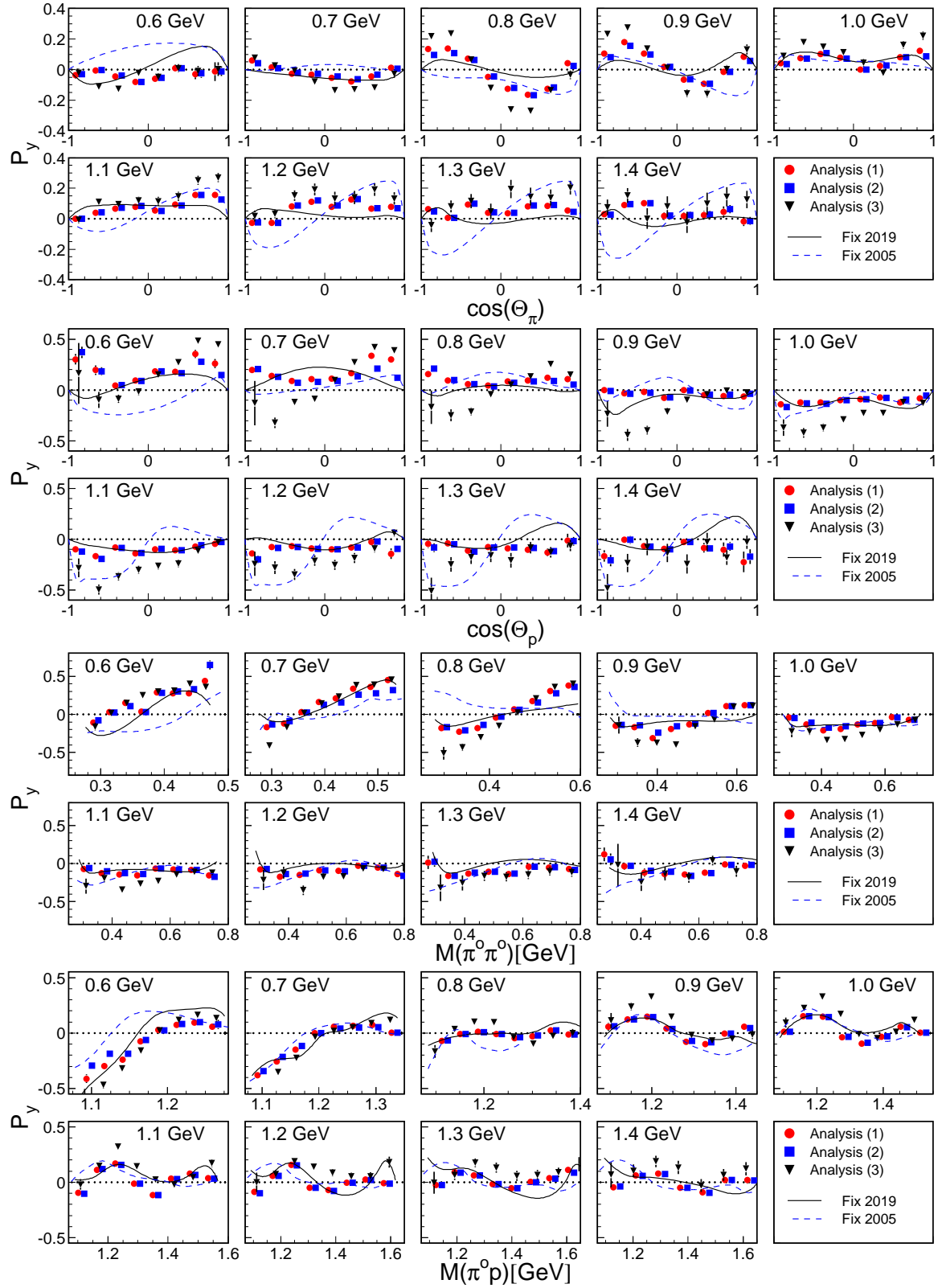


FIG. 9. (Color online) Angular and invariant mass distributions for the target asymmetry P_y of the $\gamma p \rightarrow \pi^0 \pi^0 p$ cross section for incident photon energies from 600 to 1400 MeV (bin centroids). From top to bottom results as function of pion polar angle (both pions for each event), proton polar angle, invariant mass of pion pair and invariant mass of nucleon pion pairs (two entries per event). The (red) points correspond to analysis (1), the (blue) squares to analysis (2), and the (black) triangles to analysis (3). The curves show the predictions of the isobar model [34]. The (blue) dashed curves correspond to the original 2005 version, the (black) solid curves to a refit including the new results (see text for more details).

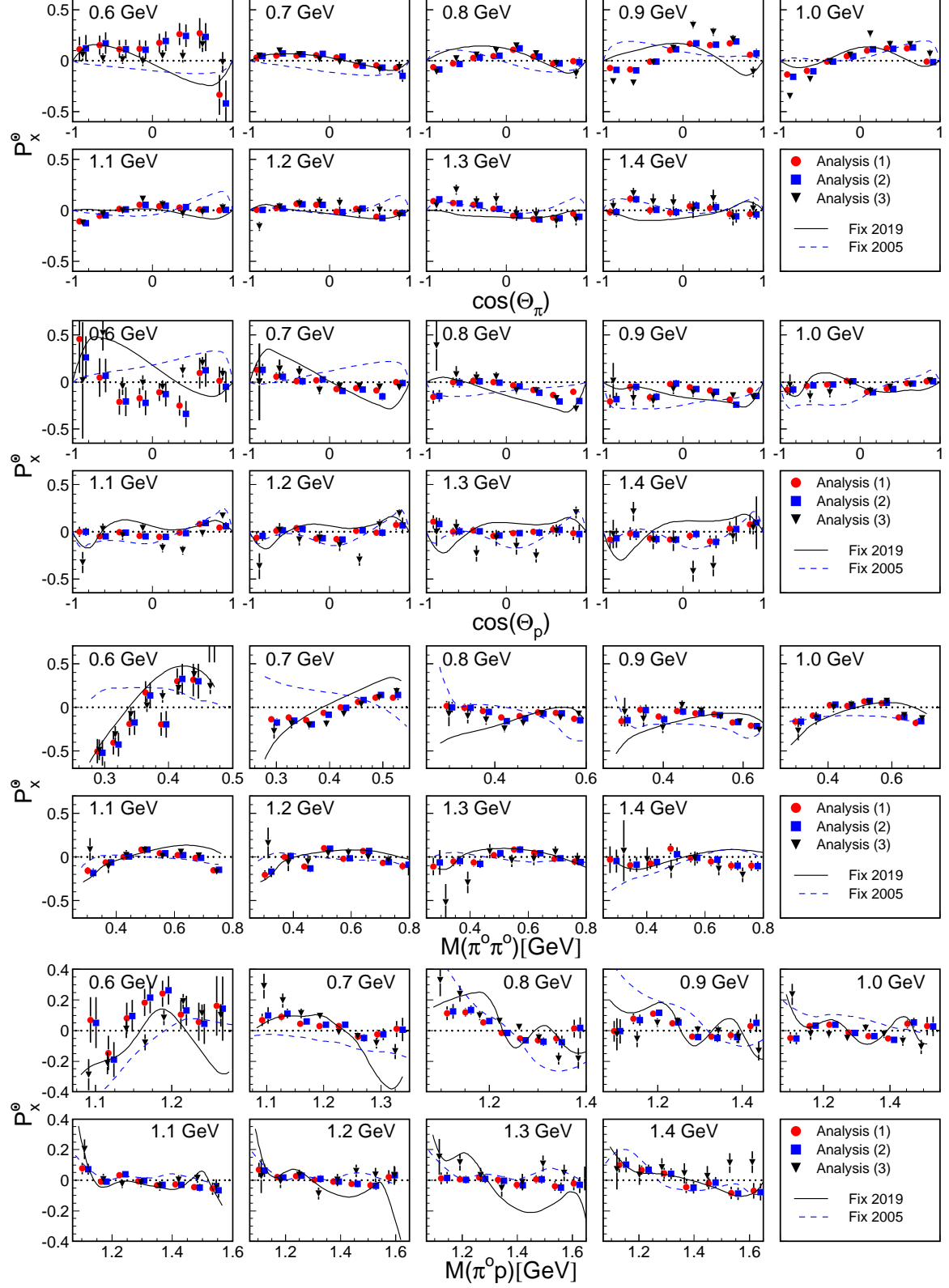


FIG. 10. (Color online) Same as in Fig. 9 for the beam-target asymmetry P_x^0 .

The carbon data was analyzed with the PID when it was compared to Run II and with the MWPCs for comparison with Run III. The agreement is reasonably good and demonstrates that the absolute calibration and the background subtraction procedure allows the correct cross section for the free $\gamma p \rightarrow p\pi^0\pi^0$ reaction to be extracted from the measurements with the solid butanol targets. Therefore, systematic effects on the asymmetries from the normalization of the cross section data and the background subtraction are not expected to be important. This can be verified from the comparison of the asymmetries extracted with the hydrogen normalization method or the carbon background subtraction (see Sec. VI).

VI. DISCUSSION OF THE RESULTS

Figures 9 - 12 show the results for the asymmetries. We follow the definitions of the asymmetries introduced in Ref. [38]. Those used in Ref. [39] may be obtained from Eqs. (2). The target asymmetries P_y and the beam-target asymmetries P_x^\odot extracted from the three different analyses are compared in Figs. 9 and 10, respectively. The results from the two analyses using the charged particle detectors and either a normalization to the measurement with the liquid hydrogen target or the subtraction of the carbon background are in quite good agreement.

The analysis with the crude proton identification by hit multiplicity agrees reasonably well with the other two results for the beam-target double asymmetry P_x^\odot (Fig. 10) for which many systematic effects cancel. Agreement for the target asymmetry P_y is also acceptable for the asymmetries as function of invariant masses and of pion angles, but not for the asymmetries as function of proton angle. In the latter case, the results not using the MWPCs suffer not only from misidentifications but also from the much worse angular resolution for the recoil protons. We have therefore discarded them in Fig. 9. Overall, the statistical precision of analysis (3) is much lower than for the other two analyses because the cut on hit-multiplicity one for the proton candidates eliminates a significant fraction of good events.

Another set of observables, P_x and P_y^\odot contribute exclusively to the distribution over the azimuthal angle ϕ_{23}^* (the angle between reaction and production plane) and vanish when integrated over this angle. These are asymmetries which due to parity conservation can only appear in three-body final states. These observables have only been analyzed with analysis (3) (i.e. proton identification with hit multiplicity and carbon background subtraction). Therefore, the control of systematic uncertainties is less good than for the other observables. On the other hand, systematic uncertainties from detector effects are less important for this observables because for a fixed angle between reaction and production plane the data are integrated over all azimuthal angles in the laboratory coordinate system so that most systematic effects

from instrumental asymmetries vanish.

The results for P_x and P_y^\odot are shown in Figs. 11 and 12. Parity conservation requires that

$$P_x(\phi) = -P_x(2\pi - \phi), \quad P_y^\odot(\phi) = -P_y^\odot(2\pi - \phi), \quad (11)$$

which is visible in the two figures (it means the asymmetries are invariant when mirrored around 2π and the sign of the ordinate is inverse).

According to the partial wave expansion of [25] these two observables and the beam-helicity asymmetry I^\odot [15] are determined by interferences of partial waves of the same parity. Therefore, in contrast to the asymmetries P_y and P_x^\odot discussed above, in this case the waves with opposite parities are added incoherently. Thus, the information contained in the data for P_x , P_y^\odot and I^\odot is complementary to those for the first two asymmetries. As may be seen, these observables have relatively large values only at low incident photon energies. With increasing energy the oscillations become smaller. There is no indication of oscillations with higher frequency (which would be characteristic for contributions from larger angular momenta).

As a theoretical basis we use an isobar model similar to that presented in Ref. [34]. The reaction amplitude consists of two main terms. The first one includes the nucleon and Δ -nucleon Born diagrams ((a) to (k) in Fig. 1). The second term, represented by the diagrams (l) and (m), contains the sum of s -channel Breit-Wigner resonances. In the calculation presented in Ref. [34] the resonance parameters, including γN coupling and partial decay widths, were taken from the Particle Data Group (PDG) compilation of Ref. [59].

In contrast to [34], in the present version of the model the resonance parameters were fitted to the data. Furthermore, besides the Born diagrams in Fig. 1 we included additional background terms in the amplitude which were not contained in the model of [34]. This takes into account the results of the analysis [14]. There, it was found that the amplitude should contain rather large fractions of the partial waves with $J^P = 3/2^\pm$, which are not reproduced by the previous analysis [34]. As is shown in [14], the background terms seem to be responsible for the steep rise of the total cross section for $\gamma p \rightarrow \pi^0\pi^0 p$ in the region below the first maximum at $W = 1500$ MeV (see Fig. 7). The major constraint of the theory is that these terms should have a smooth energy dependence.

The resulting model amplitudes, including additional background terms, were fitted to the available data for $\gamma N \rightarrow \pi\pi N$ in all charge channels in the region up to the total energy $W = 1900$ MeV. The asymmetries P_x , P_y , P_x^\odot , and P_y^\odot obtained in the present work were included in the fitting procedure. The N and Δ resonances fitted to the available $\gamma N \rightarrow \pi\pi N$ data, along with their resonance parameters are listed in Tables IV and V. For the fitting procedure the initial values of the resonance parameters were taken from the current Particle Data Group listing [60]. Since the resonance terms are proportional to the product of the electromagnetic and

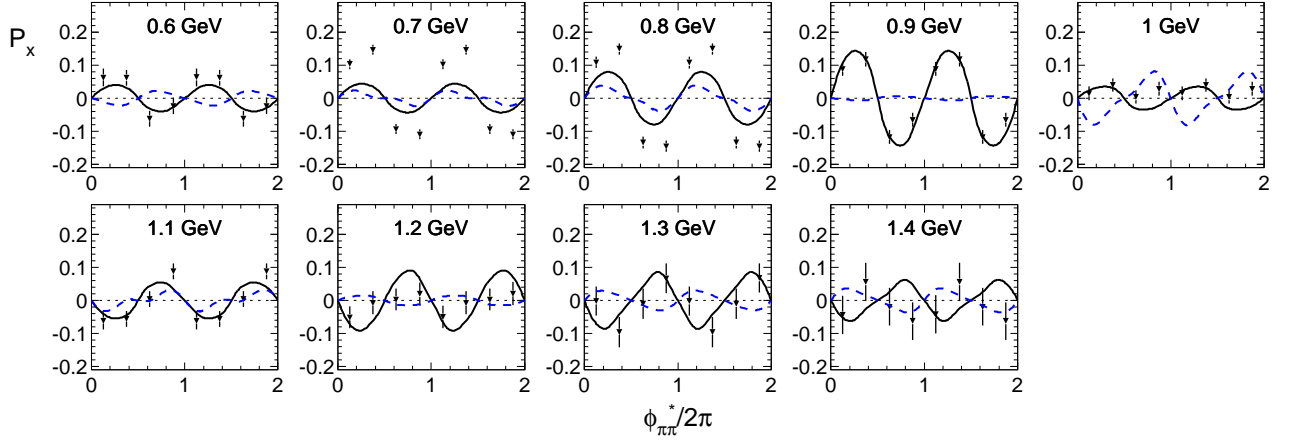


FIG. 11. (Color online) Same as in Fig.9 for the asymmetries $P_x(\phi_{\pi\pi}^*)$ from analysis (3). ($\phi_{\pi\pi}^*$ angle between production and reaction plane, see Fig. 2).

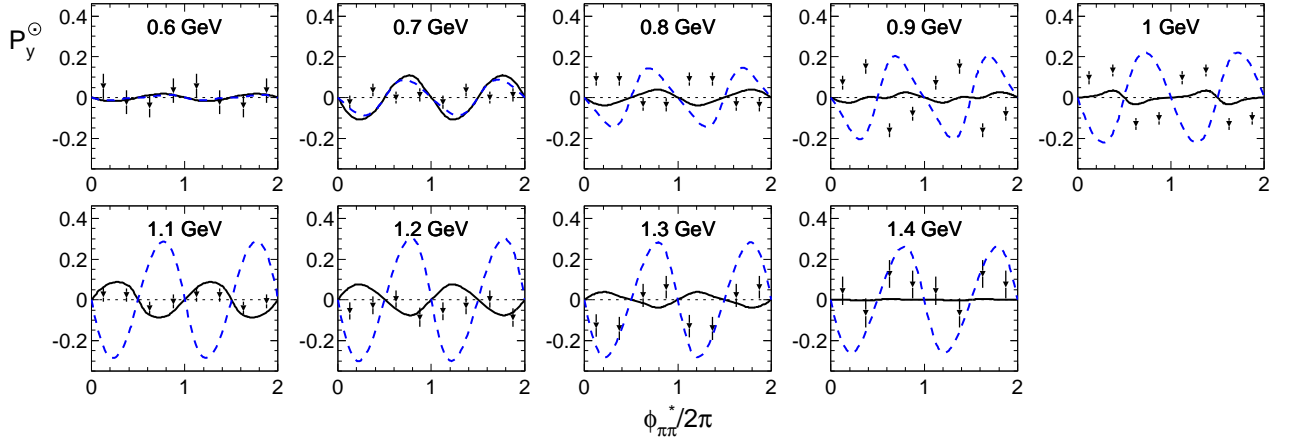


FIG. 12. (Color online) Same as in Fig.9 for the asymmetry $P_y^\circ(\phi_{\pi\pi}^*)$ from analysis (3). ($\phi_{\pi\pi}^*$ angle between production and reaction plane, see Fig. 2).

hadronic couplings in the tables the products $\sqrt{\beta_\alpha} A_{1/2}$ with $\alpha = \{\pi\Delta, \rho N, \sigma N\}$ and the ratio of the helicity amplitudes $A_{3/2}/A_{1/2}$ is given. The corresponding total cross section as well as the target and the beam-target asymmetries are shown in Figs. 7,9-12 as black solid lines.

In comparison to the analysis of [34] the new isobar model includes a larger number of resonances, especially in the high-mass range. All states with masses up to 1950 MeV and an overall status of *** were included, as well as the baryon $N(1700)3/2^-$ which according to [60] has a status of *** in the $\pi\Delta$ channel. Comparing the results for the states which were included in [34] and the present fit, one observes significant changes to their parameters. To some extent this variation is caused by the difference between their values in [59] and [60]. This is particularly the case for the ρN and σN decay modes.

The data for P_y and P_x° reveal some interesting properties which should be discussed in more detail. Firstly,

the large values of these asymmetries in the region below 1 GeV are notable, especially at energies below the $N(1520)3/2^-$ resonance. This effect is particularly pronounced for the asymmetries as function of the invariant masses of the $\pi^0\pi^0$ and $p\pi^0$ pairs. As can be shown by evaluation of P_y and P_x° (using, for example, the partial wave expansion of the t-matrix in [25]), their invariant mass distributions, after integration over the rest of the variables, are determined by the interference of partial waves with opposite parities. Therefore, the experimental results demonstrate that already at low incident photon energies contributions from both parities are important.

The interference effect between the states with opposite parities is also responsible for the asymmetry in the angular distributions of both observables (see Figs.9 and 10). It may be shown, using again the partial wave expansion of [25], that when only states of equal par-

TABLE IV. Parameters of the N -type resonances fitted to the data for $\gamma N \rightarrow \pi\pi N$ in the region up to the total center-of-mass energy $W = 1900$ MeV. M_R and Γ_{tot} are the Breit-Wigner mass and total width of a resonance. The notations β_α are used for the branching ratios $\Gamma_\alpha/\Gamma_{tot}$ with $\alpha = \{\pi\Delta, \rho N, \sigma N\}$. The total widths Γ_{tot} were not varied. Their values were taken directly from the Particle Data Group tables [60]. In the second row for each resonance the parameters from the earlier analysis [34] are given. The third row lists the corresponding numbers from the compilation of [60]. In those cases, when no estimation of $A_{1/2}^{(p)}$ and $A_{3/2}^{(p)}$ is made in [60] their values were taken from the analyses of [18] and [61] (marked with an asterisk).

$N(M_R)J^P$	M_R [MeV]	Γ_{tot} [MeV]	$\sqrt{\beta_{\pi\Delta}} A_{1/2}^{(p)}$ [$10^{-3}\text{GeV}^{-1/2}$]	$\sqrt{\beta_{\rho N}} A_{1/2}^{(p)}$ [$10^{-3}\text{GeV}^{-1/2}$]	$\sqrt{\beta_{\sigma N}} A_{1/2}^{(p)}$ [$10^{-3}\text{GeV}^{-1/2}$]	$A_{3/2}^{(p)}/A_{1/2}^{(p)}$
$N(1440)\frac{1}{2}^+$	1449	350	-46.7	-12.7	-13.4	
	1440	350	-30.4	0	-23.5	
	1440 ± 30	350 ± 100	-26.4 ± 16.0	-	-26.8 ± 9.7	
$N(1520)\frac{3}{2}^-$	1525	110	-3.98	-9.98	-1.51	-7.17
	1515	115	-8.94	-8.94	0	-7
	1515 ± 5	110 ± 10	-11.9 ± 1.5	-	-2.25 ± 1.50	-6.22 ± 1.85
$N(1535)\frac{1}{2}^-$	1538	150	42.8	37.5	32.1	
	1535	150	0	17.78	17.78	
	1530 ± 15	150 ± 25	16.6 ± 15.2	-	25.7 ± 24.7	
$N(1650)\frac{1}{2}^-$	1635	125	18.4	22.7	7.85	
	-	-	-	-	-	
	1650 ± 15	125 ± 25	15.6 ± 14.5	-	14.2 ± 15.9	
$N(1675)\frac{5}{2}^-$	1660	145	10.8	4.45	8.32	1.01
	1675	150	14.7	0	0	1.05
	1675_{-10}^{+5}	145 ± 15	9.58 ± 8.73	-	3.91 ± 4.15	1.28 ± 0.98
$N(1680)\frac{5}{2}^+$	1695	120	-1.77	-2.15	-1.30	-17.0
	1685	130	-4.68	-4.93	-5.17	-8.87
	1685 ± 5	120_{-5}^{+10}	-4.74 ± 0.14	-	-4.30 ± 0.14	-11.7 ± 6.2
$N(1700)\frac{3}{2}^-$	1732	200	31.6	17.2	6.49	-0.75
	-	-	-	-	-	-
	1720_{-70}^{+80}	200 ± 100	$34.3 \pm 30.1^*$	$25.2 \pm 20.5^*$	$11.6 \pm 14.8^*$	$-0.90 \pm 0.03^*$
$N(1710)\frac{1}{2}^+$	1711	140	40.4	11.2	2.58	
	-	-	-	-	-	
	1710 ± 30	140 ± 60	$12.2 \pm 11.1^*$	$20.6 \pm 16.4^*$	-	
$N(1720)\frac{3}{2}^+$	1723	250	77.7	24.1	5.65	1.12
	-	-	-	-	-	-
	1720_{-40}^{+30}	250_{-100}^{+150}	82.4 ± 62.3	12.2 ± 9.5	28.3 ± 30.1	$1.35 \pm 0.67^*$
$N(1900)\frac{3}{2}^+$	1920	200	21.5	0	6.09	-2.79
	-	-	-	-	-	-
	1920 ± 30	200_{-100}^{+120}	$17.0 \pm 20.6^*$	-	$4.80 \pm 6.96^*$	$-2.79 \pm 0.38^*$

ity contribute, the asymmetries $P_y(\Theta_p)$ and $P_x^\circ(\Theta_p)$ are odd functions of their arguments, so that, for instance, $P_y(\pi - \Theta_p) = -P_y(\Theta_p)$. This is not true for the measured data (see Figs. 9,10) which is further evidence that even at low incident photon energies amplitudes with both parities must contribute.

VII. SUMMARY AND CONCLUSIONS

The present work reports experimental results for the target and beam-target asymmetry for photoproduction of π^0 pairs off protons. The data were measured with a circularly polarized photon beam at the tagged-photon facility of the Mainz MAMI accelerator and a transversally polarized solid butanol target. The reaction prod-

TABLE V. Same as in Table IV for the Δ -type resonances included into the model.

$\Delta(M_R)J^P$	M_R [MeV]	Γ_{tot} [MeV]	$\sqrt{\beta_{\pi\Delta}} A_{1/2}$ [$10^{-3}\text{GeV}^{-1/2}$]	$\sqrt{\beta_{\rho N}} A_{1/2}$ [$10^{-3}\text{GeV}^{-1/2}$]	$A_{3/2}/A_{1/2}$
$\Delta(1600)\frac{3}{2}^+$	1614	250	-55.7	-19.7	0.66
	— 1570 ± 70	— 250 ± 50	— -39.7 ± 3.2	— —	— 0.778 ± 0.592
$\Delta(1620)\frac{1}{2}^-$	1615	140	-7.96	-5.61	
	1620	150	12.0	0	
	1610 ± 20	130 ± 20	35.4 ± 26.0	—	
$\Delta(1700)\frac{3}{2}^-$	1718	300	25.5	28.6	1.22
	—	—	—	—	—
	1710 ± 20	300 ± 80	71.2 ± 74.6	—	1.00 ± 0.54
$\Delta(1905)\frac{5}{2}^+$	1860	330	8.72	19.4	-1.59
	—	—	—	—	—
	1880^{+30}_{-25}	330^{+70}_{-60}	20.9 ± 11.7	—	-2.04 ± 0.01
$\Delta(1910)\frac{1}{2}^+$	1882	300	26.7	2.08	
	—	—	—	—	
	1900 ± 50	300 ± 100	14.1 ± 15.1	—	
$\Delta(1950)\frac{7}{2}^+$	1949	285	-26.3	17.3	0.87
	—	—	—	—	—
	1930^{+20}_{-15}	285 ± 50	-15.6 ± 12.9	—	1.28 ± 0.23

ucts (π^0 decay photons and recoil protons) were detected with the electromagnetic calorimeter combining the Crystal Ball and the TAPS detectors, supplemented by detectors for charged particle identification. The results represent a further piece in the puzzle to disentangle the partial wave content of the $\gamma p \rightarrow p\pi^0\pi^0$ reaction in the second and third resonance regions.

The experimental data are compared to the results of an isobar model with non-resonant background. The model of Ref. [34] disagrees significantly with the data in the threshold region. In particular the total cross section above and below the $N(1520)3/2^-$ maximum is not reproduced, obviously significant contributions are missing. In the range of photon energies between 0.8 and 1 GeV, in between the double-bump structure in the total cross section, all asymmetries deviate significantly between the model [34] and experiment.

The present data for the target and the beam-target asymmetries have been included in a new analysis of $\gamma N \rightarrow \pi\pi N$ at the energies from the threshold to $W = 1900$ MeV. Compared to the results of Ref. [34], the new solution provides a much better description of the data in the $\pi^0\pi^0 p$ channel in the entire energy range.

The measurement of further observables for this reaction is certainly necessary. Some observables (e.g. reactions with a circularly polarized photon beam and longitudinally polarized target for quasifree protons and neutrons) have already been measured and are in preparation

for publication.

ACKNOWLEDGMENTS

We wish to acknowledge the outstanding support of the accelerator group and operators of MAMI. This work was supported by Schweizerischer Nationalfonds (200020-156983, 132799, 121781, 117601), Deutsche Forschungsgemeinschaft (SFB 443, SFB 1044, SFB/TR16), the INFN-Italy, the European Community-Research Infrastructure Activity under FP7 programme (Hadron Physics, grant agreement No. 227431), the UK Science and Technology Facilities Council (ST/J000175/1, ST/G008604/1, ST/G008582/1, ST/J00006X/1, and ST/L00478X/1), the Natural Sciences and Engineering Research Council (NSERC, FRN: SAPPJ-2015-00023), Canada. A.F. acknowledges additional support from the Tomsk Polytechnic University Competitiveness Enhancement Program. This material is based upon work also supported by the U.S. Department of Energy, Office of Science, Office of Nuclear Physics Research Division, under Award Numbers DE-FG02-99-ER41110, DE-FG02-88ER40415, DE-FG02-01-ER41194, and DE-SC0014323 and by the National Science Foundation, under Grant Nos. PHY-1039130 and IIA-1358175.

-
- [1] A. Braghieri *et al.*, Phys. Lett. **B 363**, 46 (1995).
[2] F. Härter *et al.*, Phys. Lett. **B 401**, 229 (1997).
[3] B. Krusche *et al.*, Eur. Phys. J. **A 6**, 309 (1999).
[4] M. Wolf *et al.*, Eur. Phys. J. **A 9**, 5 (2000).
[5] V. Kleber *et al.*, Eur. Phys. J. **A 9**, 1 (2000).
[6] Y. Assafiri *et al.*, Phys. Rev. Lett. **90**, 222001 (2003).
[7] M. Kotulla *et al.*, Phys. Lett. **B 578**, 63 (2004).
[8] J. Ahrens *et al.*, Phys. Lett. **B 624**, 173 (2005).
[9] J. Ajaka *et al.*, Phys. Lett. **B 651**, 108 (2007).
[10] A. V. Sarantsev *et al.*, Phys. Lett. **B 659**, 94 (2008).
[11] U. Thoma *et al.*, Phys. Lett. **B 659**, 87 (2008).
[12] D. Krambrich *et al.*, Phys. Rev. Lett. **103**, 052002 (2009).
[13] F. Zehr *et al.*, Eur. Phys. J. **A 48**, 98 (2012).
[14] V. L. Kashevarov *et al.*, Phys. Rev. **C 85**, 064610 (2012).
[15] M. Oberle *et al.*, Phys. Lett. **B 721**, 237 (2013).
[16] M. Dieterle *et al.*, Eur. Phys. J. **A 51**, 142 (2015).
[17] V. Sokhoyan *et al.*, Phys. Lett. **B 746**, 127 (2015).
[18] V. Sokhoyan *et al.*, Eur. Phys. J. **A 51**, 95 (2015), Erratum: [Eur. Phys. J. **A 51**, 187 (2015)]
[19] A. Thiel *et al.*, Phys. Rev. Lett. **114**, 091803 (2015).
[20] A. Zabrodin *et al.*, Phys. Rev. **C 55**, R1617 (1997).
[21] A. Zabrodin *et al.*, Phys. Rev. **C 60**, 055201 (1999).
[22] W. Langgärtner *et al.*, Phys. Rev. Lett. **87**, 052001 (2001).
[23] S. Strauch *et al.*, Phys. Rev. Lett. **95**, 162003 (2005).
[24] M. Oberle *et al.*, Eur. Phys. J. **A 50**, 54 (2014).
[25] A. Fix and H. Arenhovel, Phys. Rev. **C 85**, 035502 (2012).
[26] B. Krusche and C. Wilkin, Prog. Part. Nucl. Phys. **80**, 43 (2015).
[27] A. Käser *et al.*, Phys. Lett. **B 748**, 244 (2015).
[28] A. Käser *et al.*, Eur. Phys. J. **A 52**, 272 (2016).
[29] V. Sokhoyan *et al.*, Phys. Rev. **C 97**, 055212 (2018).
[30] A. Käser *et al.*, Phys. Lett. **B 786**, 305 (2018).
[31] E. Gutz *et al.*, Eur. Phys. J. **A 50**, 74 (2014).
[32] L. Y. Murphy and J. M. Laget, DAPHNIA/SPhN, 96-10 (1996).
[33] J. A. Gomez Tejedor and E. Oset, Nucl. Phys. **A 600**, 413 (1996).
[34] A. Fix and H. Arenhövel, Eur. Phys. J. **A 25**, 115 (2005).
[35] A. Anisovich, E. Klempt, A. Sarantsev and U. Thoma, Eur. Phys. J. **A 24**, 111 (2005).
[36] A. Anisovich *et al.*, Eur. Phys. J. **A 48**, 15 (2012).
[37] W.T. Chiang, F. Tabakin, Phys. Rev. **C 55**, 2054 (1997).
[38] W. Roberts and T. Oed, Phys. Rev. **C 71**, 055201 (2005).
[39] A. Fix and H. Arenhovel, Phys. Rev. **C 83**, 015503 (2011).
[40] K.-H. Kaiser *et al.*, Nucl. Instrum. Methods **A 593**, 159 (2008).
[41] J. C. McGeorge *et al.*, Eur. Phys. J. **A 37**, 129 (2008).
[42] S. J. Hall *et al.*, Nucl. Instrum. Methods **A 368**, 698 (1996).
[43] I. Anthony *et al.*, Nucl. Instrum. Methods **A 310**, 230 (1991).
[44] A. Starostin *et al.*, Phys. Rev. **C 64**, 055205 (2001).
[45] R. Novotny, IEEE Trans. Nucl. Sci. **38**, 379 (1991).
[46] A. R. Gabler *et al.*, Nucl. Instrum. Methods **A 346**, 168 (1994).
[47] D. Watts, Proc. of the 11th International Conference on Calorimetry in Particle Physics, Perugia, Italy, 2004, edited by C. Cecchi, P. Cenci, P. Lubrano, and M. Pepe (World Scientific, Singapore, 2005, p. 560)
[48] G. Audit *et al.*, Nucl. Instr. Meth. **A301**, 473 (1991).
[49] S. Prakhov *et al.*, Phys. Rev. **C 79**, 035204 (2009).
[50] E. F. McNicoll *et al.*, Phys. Rev. **C 82**, 035208 (2010).
[51] D. Werthmüller *et al.*, Phys. Rev. **C 90**, 015205 (2014).
[52] L. Witthauer *et al.*, Phys. Rev. **C 95**, 055201 (2017).
[53] M. Dieterle *et al.*, Phys. Rev. **C 97**, 065205 (2018).
[54] H. Olsen and L. C. Maximon, Phys. Rev. **114**, 887 (1959).
[55] A. Thomas, Eur. Phys. J. Special Topics **198**, 171 (2011).
[56] Y. Maghrbi *et al.* Phys. Lett. **B 69**, (2013).
[57] V.L. Kashevarov *et al.*, Eur. Phys. J. **A 42**, 141 (2009).
[58] S. Agostinelli *et al.*, Nucl. Instr. Meth. **A 506**, 250 (2003).
[59] D.E. Groom *et al.*, (Particle Data Group), Eur. Phys. J. **C 15**, 1 (2000).
[60] M. Tanabashi *et al.*, (Particle Data Group), Phys. Rev. **D 98**, 030001 (2018).
[61] A. V. Anisovich, R. Beck, E. Klempt, V. A. Nikonov, A. V. Sarantsev and U. Thoma, Eur. Phys. J. **A 48**, 15 (2012).